



CHORUS

This is the accepted manuscript made available via CHORUS. The article has been published as:

Enhanced spin-triplet pairing in magnetic junctions with s-wave superconductors

Thomas Vezin, Chenghao Shen, Jong E. Han, and Igor Žutić

Phys. Rev. B **101**, 014515 — Published 31 January 2020

DOI: [10.1103/PhysRevB.101.014515](https://doi.org/10.1103/PhysRevB.101.014515)

Enhanced spin-triplet pairing in magnetic junctions with s-wave superconductors

Thomas Vezin,^{1,2} Chenghao Shen,¹ Jong E. Han,¹ and Igor Žutić^{1,2,*}

¹*Department of Physics, University at Buffalo, State University of New York, Buffalo, NY 14260, USA*

²*Laboratoire des Solides Irradiés, Ecole Polytechnique, Université Paris-Saclay, F-91767 Palaiseau Cedex, France*

A common path to superconducting spintronics, Majorana fermions, and topologically-protected quantum computing relies on spin-triplet superconductivity. While naturally occurring spin-triplet pairing is elusive and even common spin-triplet candidates, such as Sr_2RuO_4 , support alternative explanations, proximity effects in heterostructures can overcome these limitations. It is expected that robust spin-triplet superconductivity in magnetic junctions should rely on highly spin-polarized magnets or complex magnetic multilayers. Instead, we predict that the interplay of interfacial spin-orbit coupling and the barrier strength in simple magnetic junctions, with only a small spin polarization and s-wave superconductors, can lead to nearly complete spin-triplet superconducting proximity effects. This peculiar behavior arises from an effective perfect transparency: interfacial spin-orbit coupling counteracts the native potential barrier for states of a given spin and wave vector. We show that the enhanced spin-triplet regime is characterized by a huge increase in conductance magnetoanisotropy, orders of magnitude larger than in the normal state.

I. INTRODUCTION

Realizing equal-spin triplet superconductivity provides an important platform for implementing superconducting spintronics and topologically-protected Majorana bound states (MBS) [1–7]. While naturally occurring triplet pairing remains elusive [8–11], transforming materials through proximity effects [12] offers a promising path to tailor desired forms of superconducting states [13–17].

For superconducting spintronics equal-spin triplet supports pure spin currents and the coexistence of superconductivity and ferromagnetism through long-range superconducting proximity effects in ferromagnet/superconductor (F/S) junctions [16–18]. Such junctions typically rely on multiple ferromagnetic and superconducting regions [16, 17, 19–21], complex ferromagnets with spiral magnetization [22], or complete spin polarization in half-metallic ferromagnets [23–25].

With alternative paths towards spin-triplet pairing, where interfacial spin-orbit coupling (SOC) could relax the requirement of a complex magnetic structure, it is expected that both a strong spin polarization and strong SOC are needed [26–29]. However, in a simple F/S junction as depicted in Fig. 1, we reveal that for nearly complete spin-triplet proximity-induced superconductivity even weakly spin-polarized ferromagnet and smaller SOC could be desirable. Our findings could complement the paths towards MBS where proximity-induced spin-triplet pairing is sought through strong SOC and half-metallic ferromagnets [15, 30–32].

A microscopic understanding of a superconducting proximity effect is obtained from the process of Andreev reflection at interfaces with superconductors where an electron is reflected backwards and converted into a hole with opposite charge and spin. This implies the doubling of the normal state conductance [33] since two electrons are transferred across the interface into the S region

where they form a spin-singlet Cooper pair. Unlike this conventional Andreev reflection, a spin-active interface with interfacial spin-flip scattering also yields Andreev reflection with an equal spin of electrons and holes [34], responsible for spin-triplet pair correlations [16].

Following this introduction, in Sec. II we describe the Hamiltonian and scattering states for F/S junctions. In Sec. III we provide conductance calculations that support surprising trends for interfacial spin-triplet superconductivity and explain how simple normal-state transport analysis can provide helpful guidance. Our conclusions address related experiments and open questions.

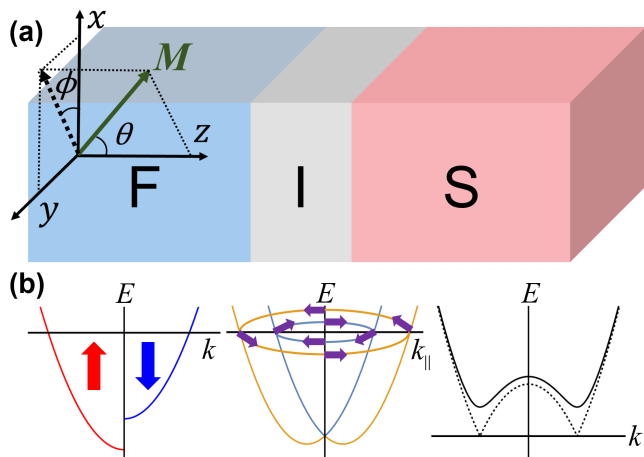


FIG. 1. Ferromagnet/superconductor (F/S) junction, F and S separated by a flat interface (I) with potential and Rashba spin-orbit scattering (SOC). \mathbf{M} is the magnetization and the current flows normal to I. (b) Schematic band structure in each region. Spin are denoted by arrows: In the F region red (blue) for parallel (antiparallel) to \mathbf{M} ; with interfacial SOC, spins are parallel to the interface and \perp to the in-plane component of the momentum, k_{\parallel} . Excitation picture in the S region, the dashed line shows the normal state dispersion.

II. HAMILTONIAN AND SCATTERING STATES

We consider ballistic F/S junction, depicted in Fig. 1, having a flat interface (I) at $z = 0$ with potential and Rashba SOC scattering [35]. We generalize the Blonder-Tinkham-Klapwijk formalism [33, 36, 37] to solve Bogoliubov-de Gennes equation for quasiparticle states $\Psi(\mathbf{r})$ with energy E [38],

$$\begin{pmatrix} \hat{H}_e & \Delta\Theta(z)I_{2\times 2} \\ \Delta^*\Theta(z)I_{2\times 2} & \hat{H}_h \end{pmatrix} \Psi(\mathbf{r}) = E\Psi(\mathbf{r}), \quad (1)$$

where the single-particle Hamiltonian for electrons is,

$$\hat{H}_e = -\frac{\hbar^2}{2}\nabla\frac{1}{m(z)}\nabla - \mu(z) - \frac{\Delta_{xc}}{2}\mathbf{m}\cdot\hat{\sigma}\Theta(-z) + \hat{H}_B, \quad (2)$$

and for holes $\hat{H}_h = -\hat{\sigma}_y\hat{H}_e^*\hat{\sigma}_y$. The interfacial scattering is modeled by delta-like potential barrier,

$$\hat{H}_B = [V_0d + \alpha(k_y\hat{\sigma}_x - k_x\hat{\sigma}_y)]\delta(z). \quad (3)$$

These terms contain the effective mass $m(z)$, the chemical potential $\mu(z)$, and the exchange spin splitting Δ_{xc} . Magnetization, \mathbf{M} , as shown in Fig. 1, has orientation $\mathbf{m} = (\sin\theta\cos\phi, \sin\theta\sin\phi, \cos\theta)$, $\hat{\sigma}$ are Pauli matrices, and \mathbf{k} is wave vector. The interface is characterized by an effective barrier height V_0 and width d and the Rashba SOC with strength α , due to structure inversion asymmetry [35]. The s -wave superconductor is described by the constant pair potential Δ . A complementary diffusive regime is extensively studied, including calculating spin-triplet correlations [39–43].

Since the in-plane wave vector \mathbf{k}_{\parallel} is conserved, the scattering states for incident spin σ electron are given by $\Psi_{\sigma}(\mathbf{r}) = e^{i\mathbf{k}_{\parallel}\cdot\mathbf{r}_{\parallel}}\psi_{\sigma}(z)$ in a four-component basis [34] where the “bar” symbol denotes the spin-flip contribution

$$\psi_{\sigma}(z) = \begin{cases} \chi_{\sigma}^e e^{ik_{\sigma}^e z} + a_{\sigma}\chi_{-\sigma}^h e^{ik_{-\sigma}^h z} + b_{\sigma}\chi_{\sigma}^e e^{-ik_{\sigma}^e z} + \bar{a}_{\sigma}\chi_{\sigma}^h e^{ik_{\sigma}^h z} + \bar{b}_{\sigma}\chi_{-\sigma}^e e^{-ik_{-\sigma}^e z} & \text{for } z < 0, \\ c_{\sigma} \begin{pmatrix} u \\ 0 \\ v \\ 0 \end{pmatrix} e^{iq^e z} + d_{\sigma} \begin{pmatrix} v \\ 0 \\ u \\ 0 \end{pmatrix} e^{-iq^h z} + \bar{c}_{\sigma} \begin{pmatrix} 0 \\ u \\ 0 \\ v \end{pmatrix} e^{iq^e z} + \bar{d}_{\sigma} \begin{pmatrix} 0 \\ v \\ 0 \\ u \end{pmatrix} e^{-iq^h z} & \text{for } z > 0. \end{cases} \quad (4)$$

In the F region, the eigenspinors for electrons and holes are $\chi_{\sigma}^e = (\chi_{\sigma}, 0)^T$ and $\chi_{\sigma}^h = (0, \chi_{-\sigma})^T$ with

$$\chi_{\sigma} = (1/\sqrt{2})\left(\sigma\sqrt{1+\sigma\cos\theta}e^{-i\phi}, \sqrt{1-\sigma\cos\theta}\right)^T, \quad (5)$$

where $\sigma = 1(-1)$ refer to spin parallel (antiparallel) to \mathbf{M} and the z -components of the wave vector are $k_{\sigma}^{e(h)} = \sqrt{k_F^2 + (2m_F/\hbar^2)[(-)E + \sigma\Delta_{xc}/2] - k_{\parallel}^2}$, with a spin-averaged Fermi wave vector, k_F [44]. At an interface, with conserved \mathbf{k}_{\parallel} , the eigenspinors of the barrier Hamiltonian \hat{H}_B in the helicity basis are given by [45, 46],

$$\chi_{\pm} = \frac{1}{\sqrt{2}} \begin{pmatrix} 1 \\ \mp ie^{i\gamma} \end{pmatrix}, \quad (6)$$

where where γ is the angle between \mathbf{k}_{\parallel} and $\hat{\mathbf{k}}_x$.

In the S region, coherence factors, u, v , satisfy $u^2 = 1 - v^2 = (1 + \sqrt{E^2 - \Delta^2}/E)/2$, while the z -components of the wave vector are $q^{e(h)} = \sqrt{q_F^2 + (-)(2m_S/\hbar^2)\sqrt{E^2 - \Delta^2} - k_{\parallel}^2}$, with q_F the Fermi wave vector. Similar to Snell’s law [44], for a large k_{\parallel} these z -components can become imaginary representing evanescent states which carry no net current. The vanishing of evanescent states at infinity requires $\text{Im}[k_{\sigma}^h] < 0$, so the sign of the z -component of the wave vectors needs to be chosen correctly.

III. CONDUCTANCE IN F/S JUNCTIONS

From the charge current conservation, we can express zero-temperature conductance at applied bias, V ,

$$G(V) = \sum_{\sigma} \int \frac{dk_{\parallel}}{2\pi k_F^2} [1 + R_{\sigma}^h(-eV) - R_{\sigma}^e(eV)], \quad (7)$$

normalized by the Sharvin conductance $G_{\text{Sh}} = e^2 k_F^2 A / (2\pi\hbar)$ [35], where A is the interfacial area. Only the probability amplitudes from the F region are needed, for Andreev $R_{\sigma}^h = \text{Re}[(k_{-\sigma}^h/k_{\sigma}^e)|a_{\sigma}|^2 + (k_{\sigma}^h/k_{\sigma}^e)|\bar{a}_{\sigma}|^2]$ and specular reflection $R_{\sigma}^e = \text{Re}[|b_{\sigma}|^2 + (k_{-\sigma}^e/k_{\sigma}^e)|\bar{b}_{\sigma}|^2]$.

We focus on the zero-bias conductance, $G(0)$, where there is no quasiparticle transmission and, from the probability conservation [34, 38], can be expressed using AR such that in Eq. (7) the integration kernel is $2[R_{\sigma}^h(0)]$. The total $G(0)$ can be decomposed into four processes [see Eq. (4) and Fig. 2]: Conventional and spin-flip AR for spin-up (spin-down) \uparrow (\downarrow) incident electrons corresponding, respectively, to the spin-singlet and spin-triplet superconducting correlations at the interface. It is convenient to introduce spin polarization $P = \Delta_{xc}/2\mu_F$, and dimensionless parameters for barrier strength and Rashba SOC,

$$Z = V_0d\sqrt{m_F m_S}/(\hbar^2\sqrt{k_F q_F}), \quad \lambda = 2\alpha\sqrt{m_F m_S}/\hbar^2, \quad (8)$$

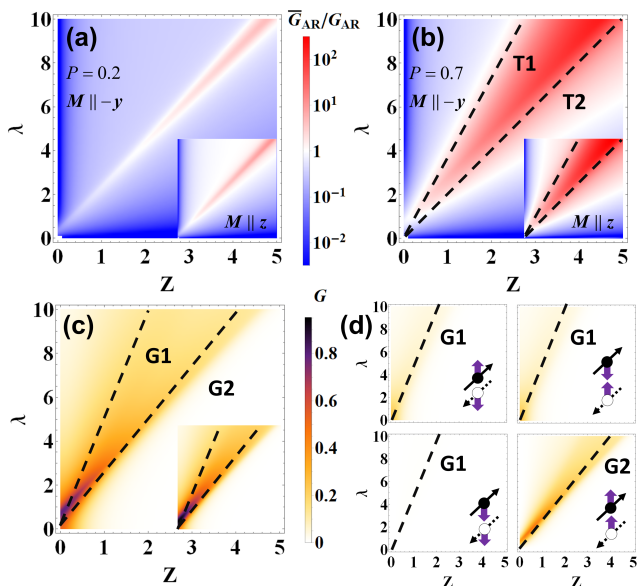


FIG. 2. The conductance ratio between the spin-flip and conventional Andreev reflection as a function of barrier potential Z and Rashba SOC strength λ for spin polarization (a) $P = 0.2$, (b) $P = 0.7$ (b) with in-plane \mathbf{M} . The insets: out-of-plane \mathbf{M} . (c) The total conductance as a function of Z and λ for in-plane and out-of-plane (inset) \mathbf{M} with $P = 0.7$ and (d) its contributions from different processes, solid (dashed) arrows: incoming electrons (reflected holes), violet arrows: spin parallel (up) and antiparallel (down) to \mathbf{M} .

respectively. As we present trends for a large parameter space, unless otherwise specified, we will consider the case for $m_F = m_S = m$ and $k_F = q_F$.

In Figs. 2(a) and (b) we show the conductance ratio between the spin-flip and conventional AR, $\bar{G}_{\text{AR}}/G_{\text{AR}}$, our proxy for singlet and triplet interfacial pairing, as function of the barrier strength and SOC. Remarkably, $\bar{G}_{\text{AR}}/G_{\text{AR}} \gg 1$, even for a small spin polarization, $P = 0.2$, a nearly complete triplet pairing is possible, $> 90\%$ (96%) for in-plane (out-of-plane) \mathbf{M} . A striking enhancement of the triplet contribution is feasible for a wide range of barrier strengths, accompanied with a suitable SOC. As shown in Fig. 2, the triangle region of this dominance increases considerably for a larger $P = 0.7$ and it is approximately delimited with lines T1 and T2,

$$\text{T1: } \lambda = 2Z/\sqrt{1-P}, \quad \text{T2: } \lambda = 2Z, \quad (9)$$

excluding the half-metals, $P = 1$. Our findings suggest that even simple s -wave junctions with only one magnetic region of a small P and interfacial SOC can support robust spin-triplet currents. These trends are also preserved for an out-of-plane \mathbf{M} [Figs. 2(a), (b) inset].

To explore this peculiar behavior and the origin of the triangle region with enhanced triplet pairing, in Fig. 2(c) we consider the total G for $P = 0.7$ showing G1 and G2 which denote local maxima in G . This high- G region, delimited by G1,2, shows a similarity, but not complete

overlap with the enhanced triplet region. Such a relatively high-subgap G is in contrast to the common expectation that for a strong barrier ($Z \gg 1$) normal metal/S (N/S) junction would resemble a tunnel contact with a small interfacial transparency $T = 1/(1 + Z^2) \ll 1$ [33].

For highly-polarized F region, $P = 0.7$, conventional AR is strongly suppressed [35, 47]. G for such F/S junction should be even lower than for the N/S counterpart with the same large Z . A striking discrepancy with these expectations comes from the neglect of the SOC and unconventional AR. Even for a strongly-polarized F region, high G is compatible with large Z and strong SOC. In the opposite regime of no SOC ($\lambda \rightarrow 0$), the triplet component will vanish [Fig. 2(b)], but there is still a region with only small SOC, $\lambda \sim 0.5$, and a large triplet pairing.

In Fig. 2(d) we resolve G for four AR processes, responsible for proximity effects, to examine the evolution of relative contribution of singlet and triplet pairing with interfacial parameters. While local maxima of G along G1 arise from singlet contributions $|\uparrow\downarrow\rangle, |\downarrow\uparrow\rangle$ and a tiny minority spin-triplet pairing $|\downarrow\downarrow\rangle$, G2 occurs from majority spin-triplet pairing $|\uparrow\uparrow\rangle$. This opens a path to tailor junctions parameters which would selectively remove the singlet contribution and ensure that transport properties are dominated by (majority) spin-triplet pairing.

The origin the dominant triplet contribution bounded by the T1 and T2 can be traced to the normal-state properties in the corresponding F/N junction by taking $\Delta = 0$. This is further shown in Appendix A. At the interface (barrier region), the dispersion relation is,

$$E = \hbar^2(k_z^2 + k_{\parallel}^2)/2m - \mu + V_0 \pm \alpha k_{\parallel}/d, \quad (10)$$

where the energy band is split due to SOC [see Fig. 1(b)] and shifted up by the barrier potential (assuming $V_0 > 0$, but $V_0 < 0$ gives the same results). A spinor of an incident electron with \mathbf{k}_{\parallel} can be decomposed into barrier eigenspinors, $|\chi_{\sigma}\rangle = \langle\chi_{+}|\chi_{\sigma}\rangle|\chi_{+}\rangle + \langle\chi_{-}|\chi_{\sigma}\rangle|\chi_{-}\rangle$, where χ_{\pm} from Eq. (6) has helicity ± 1 . We recognize that these two helicities for outer/inner band have *inequivalent* effective barriers, see Appendix A,

$$Z_{\text{eff}}^{+} = Z + \frac{\lambda k_{\parallel}}{2\sqrt{k_F q_F}}, \quad Z_{\text{eff}}^{-} = Z - \frac{\lambda k_{\parallel}}{2\sqrt{k_F q_F}}. \quad (11)$$

Since $Z, \lambda k_{\parallel}/(2\sqrt{k_F q_F}) \geq 0$, for positive helicity the barrier is enhanced, $Z_{\text{eff}}^{+} \geq Z$. However, for negative helicity, at $Z = \lambda k_{\parallel}/(2\sqrt{k_F q_F})$, Z_{eff}^{-} becomes effectively completely transparent and gives a dramatically increased G .

The effect of this selective barrier transparency and the resulting open channels for a given \mathbf{k}_{\parallel} and σ , can be clearly seen in Fig. 3(a). The dominant contribution to k_{\parallel} -resolved conductance comes from the open channels located on the circle of radius,

$$k_{\parallel}^0 = (2Z/\lambda)\sqrt{k_F q_F}. \quad (12)$$

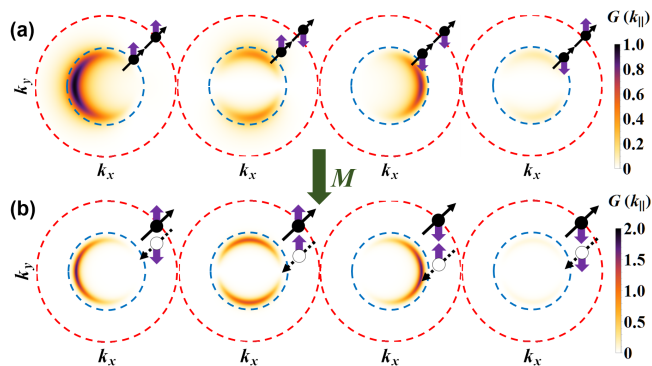


FIG. 3. Normalized σ and k_{\parallel} -resolved G for different scattering processes in (a) F/N and (b) F/S junctions with $P = 0.7$, $Z = 4.4$, $\lambda = 20$, $\mathbf{M} \parallel -y$. Parallel (antiparallel) purple arrows schematically denote no spin flip in the first and third panels. The spin of an incident electron is collinear with \mathbf{M} . The red (blue) circle has a radius k_F (k_{\downarrow}) of the spin-averaged and spin-down Fermi wave vectors, respectively.

Focusing on the case $k_F = q_F$, to maximize G for the F/N junction, there are several contributing factors. (i) The number of open channels, $N(Z, \lambda)$, should be large. Located on the circle of radius k_{\parallel}^0 , their number increases with the perimeter, $N(Z, \lambda) \propto k_{\parallel}$. (ii) The open channels should exclude evanescent waves for large k_{\parallel} , not contributing to G . This range of k_{\parallel} follows from the Snell's law [44], for incident \downarrow (\uparrow) electron: $k_{\parallel} \leq k_{\downarrow}$ ($k_{\parallel} \leq k_F$). In the extreme cases, $k_{\parallel}^0 = k_{\downarrow}$ and $k_{\parallel}^0 = k_F$, we recover exactly T1 and T2 from Eq. (9). (iii) With spin-momentum locking of interfacial helical states, an enhanced F/N transmission depends also on the spin matching with the incident spin, in addition to the usual wave vector matching [34], see Appendix A.

From these considerations we can understand why, instead of having full circles of open channels, in Fig. 3 we see crescent-like shapes. For the equal-spin transmissions in Fig. 3(a) [first (third) process from the left], their maxima are reached at $\mathbf{k}_{\parallel} = (\mp k_{\parallel}^0, 0)$, where the eigen-spin at the interface matches the spins of both incoming and outgoing particles. The different magnitudes of the maxima (between the first and third process), are due to the different matching of the wave vectors between the incoming and outgoing particles in these two processes.

This picture can be additionally verified from a simple, but accurate, analytical description of F/N transmission using selective junction transparency. The transmission decomposed into spin-conserving and spin-flip part,

$$T_{\sigma} = T_{\sigma\sigma} + T_{\sigma-\sigma}, \quad (13)$$

yields, as discussed in Appendix A,

$$T_{\sigma\sigma} \propto [1 - \sigma \cos(\gamma - \phi)]^2, \quad (14)$$

$$T_{\sigma-\sigma} \propto \sin^2(\gamma - \phi), \quad (15)$$

confirming $\pi/2$ and π symmetry from Fig. 3(a), respec-

tively. Here previously given angles ϕ and γ describe the in-plane orientation of \mathbf{M} and the barrier eigenspinor.

This analysis applies also to F/S junctions, revealing in Fig. 3(b) a similar angular dependence of k_{\parallel} -resolved G due to conventional and spin-flip AR. Some quantitative modifications from the F/N case, can be understood already without SOC due to a different condition for a perfect F/S transparency at normal incidence were all the wave vectors can be unequal $k_{\uparrow}k_{\downarrow} = q_F^2$ [34, 44]. For F/S junctions the condition for open channels again requires $k_{\parallel} \leq k_F$ which excludes the evanescent states in AR. The only subtlety is $G_{\uparrow\uparrow}$ from spin-flip AR where we could expect that $k_F < k_{\parallel} \leq k_{\uparrow}$ is also possible. However, such a large k_{\parallel} would result in a strongly decaying wave vector in the S region [recall the expression for $q^{e(h)}$] with its inverse smaller than the BCS coherence length and thus render ineffective any contribution for spin-majority pairing with $k_{\parallel} \leq k_F$. This provides a guidance for a choice of junction parameters giving an enhanced spin-triplet pairing between the lines T1 and T2 in Eq. (9), even for previously unexpected regimes with only a small P .

IV. DISCUSSION AND CONCLUSIONS

In addition to directly measuring the spin structure of G or spin current, an experimental test of our predictions for enhanced spin-triplet pairing could be realized through probing magnetic anisotropy of conductance in F/S junctions, referred to as magnetic anisotropic Andreev reflection (MAAR) [38]. MAAR and its better studied normal-state analog, tunneling anisotropic magnetoresistance (TAMR) [45, 48], can be expressed for out-of-plane rotation of \mathbf{M} [Fig. 1(a)] as [38]

$$\text{TAMR}(\theta), \text{MAAR}(\theta) = [G(0) - G(\theta)]/G(0), \quad (16)$$

where angle θ is between \mathbf{M} and the interface normal. From the evolution of MAAR, shown in Figs. 4(a) and (b) for $P = 0.2$ and $P = 0.7$, we see that it closely follows the trends of the enhanced majority spin-triplet pairing from Figs. 2(a) and (b). It is this spin-triplet component that is responsible for a large increase of MAAR compared to TAMR, in the normal state, Figs. 4(a), (c), (d). Even for $P = 0.2$ the resulting increase can reach an order of magnitude and become much larger for $P = 0.7$ where it was recently measured in all-epitaxial Fe/MgO/V junctions [49] to exceed 1000! Rather than change MAAR to TAMR by increasing the temperature above the critical temperature (for vanadium ~ 4 K), experimentally it is more convenient to reach the normal state by increasing the bias, $V > \Delta$ at a fixed temperature [49].

Such Fe/MgO/V junctions simplify the analysis of the observed magnetic anisotropy since they have two stable zero-field ($B = 0$) states with mutually orthogonal \mathbf{M} : in-plane and out-of-plane [49, 50]. This removes common complications in other F/S junction by

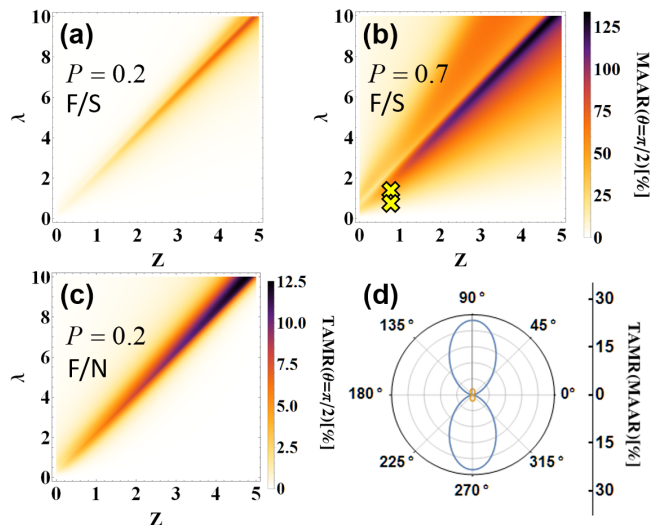


FIG. 4. Amplitude of out-of-plane magnetoanisotropic Andreev reflection (MAAR) as a function of interface parameters Z and λ for (a) $P = 0.2$ and (b) $P = 0.7$. (c) The corresponding tunneling anisotropic magnetoresistance (TAMR) when superconducting gap vanishes for $P = 0.2$. (d) A comparison between out-of-plane TAMR (yellow) and MAAR (blue), $P = 0.2$, $Z = 5$ and $\lambda = 10.2$.

decoupling the influence of the B -field required for rotating \mathbf{M} which could alter the magnitude of magnetic anisotropy and create spurious effects from vortices. Junction parameters $Z = 0.83$ ($V_0 = 0.3$ eV, $d=17$ nm), $\lambda = 0.79, 1.44$ ($\alpha = 5.5$ eVÅ²), describing two measured Fe/MgO/V samples with MAAR of 10-20 % (TAMR only ~ 0.01 %) [49] are marked in Fig. 4(b). This small SOC, $\lambda \sim 1$, smaller than in Fe/GaAs/Au TAMR studies [48], is already sufficient for a dominant triplet pairing.

While we employ a simple approach which naturally suggests a number of generalizations, from inclusion of the self-consistent pair potential, finite B -fields, study of critical temperature, noncentrosymmetric superconductors [51], more complex barrier description [52–57], its transparency already reveals several important trends and can support peculiar experimental observation of a giant MAAR [49]. Our implications for enhanced triplet pairing and MAAR detection could also be relevant for two-dimensional materials, as supported by the work in Refs. [58, 59]. Another extension of this work could include the role of magnetic textures which themselves result in synthetic spin-orbit coupling and could be used to control Majorana bound states [60–69].

Similar to the advances in realizing large magnetoresistive effect, not by employing complex ferromagnets with nearly complete spin polarization, but rather choosing a suitable nonmagnetic barrier [70, 71], our findings suggest what could constitute a suitable interface to realize enhanced spin-triplet proximity. In particular, to further enhance such triplet pairing with only a very small spin

polarization of a ferromagnet, a challenge would be to design interfaces which could simultaneously provide a large spin-orbit coupling and large potential barrier.

ACKNOWLEDGMENTS

We thank Petra Högel, Farkhad Aliev, Niladri Banerjee, Matthias Eschrig, and Carlos Egues, for valuable discussions. This work is supported by Department of Energy, Basic Energy Sciences Grant DE-SC0004890 and the UB Center for Computational Research.

APPENDIX A: ANALYTICAL SOLUTION FOR F/N JUNCTIONS

The Hamiltonian for the ferromagnet/normal metal (F/N) junction with interfacial Rashba spin-orbit coupling (SOC) can be written from Eqs. (2) and (3) [38]. Similar to the main text, we focus on the case of equal effective mass $m(z) \equiv m$ and chemical potential $\mu(z) \equiv \mu$, in the F and S region. Having these quantities unequal was considered in Ref. [34]. The corresponding scattering states are given by $\Phi_\sigma(\mathbf{r}) = e^{i\mathbf{k}_\parallel \cdot \mathbf{r}_\parallel} \psi_\sigma(z)$, where $\sigma = 1(-1)$ refer to spin parallel (antiparallel) to \mathbf{M} with

$$\psi_\sigma(z) = \begin{cases} \chi_\sigma e^{ik_\sigma z} + r_{\sigma\sigma} \chi_\sigma e^{-ik_\sigma z} \\ \quad + r_{\sigma-\sigma} \chi_{-\sigma} e^{-ik_{-\sigma} z}, & z < 0, \\ t_{\sigma\sigma} \chi_\sigma e^{ik_N z} + t_{\sigma-\sigma} \chi_{-\sigma} e^{ik_N z}, & z > 0, \end{cases} \quad (17)$$

where the spinors χ_σ are given from Eq. (5), while the z -component of the wave vectors are $k_\sigma = \sqrt{k_F^2 (1 + \sigma P) - k_\parallel^2}$, $k_N = \sqrt{k_F^2 - k_\parallel^2}$, with spin polarization $P = \Delta_{xc}/2\mu$, where Δ_{xc} is the exchange spin splitting. We use dimensionless barrier strength and Rashba SOC, Z and λ , from Eqs. (8). In scattering coefficients, $r_{\sigma\sigma}$ ($r_{\sigma-\sigma}$) denote the reflection without (with) spin flip, while $t_{\sigma\sigma}$ ($t_{\sigma-\sigma}$) denote the transmission without (with) spin flip.

Decomposing the incident state in the helicity basis from Eq. (6), $\{\chi_-, \chi_+\}$, the scattering wave function can be rewritten as $\psi_\sigma(z) = \langle \chi_+ | \chi_\sigma \rangle \psi_\sigma^{(+)}(z) + \langle \chi_- | \chi_\sigma \rangle \psi_\sigma^{(-)}(z)$ with

$$\psi_\sigma^{(\pm)}(z) = \begin{cases} \chi_\pm e^{ik_\sigma z} + r_{\sigma\sigma}^{(\pm)} \chi_\sigma e^{-ik_\sigma z} \\ \quad + r_{\sigma-\sigma}^{(\pm)} \chi_{-\sigma} e^{-ik_{-\sigma} z}, & z < 0, \\ t_{\sigma\sigma}^{(\pm)} \chi_\sigma e^{ik_N z} + t_{\sigma-\sigma}^{(\pm)} \chi_{-\sigma} e^{ik_N z}, & z > 0, \end{cases} \quad (18)$$

where all the coefficients are split into two parts. For example, $t_{\sigma\sigma'} = \langle \chi_+ | \chi_\sigma \rangle t_{\sigma\sigma'}^{(+)} + \langle \chi_- | \chi_\sigma \rangle t_{\sigma\sigma'}^{(-)}$ denotes the transmission coefficient for scattering without ($\sigma' = \sigma$) or with spin-flip ($\sigma' = -\sigma$). When the barrier potential and SOC are relatively large, the transmission coefficient

$t_{\sigma\sigma'}^{(+)}$ from $\psi_{\sigma'}^{(+)}$ (z) will always be suppressed since the effective barrier Z_{eff}^+ cannot be reduced, see Eq. (11). As a result, the transmission can be approximately written as

$$T_{\sigma\sigma'} = \text{Re} \left[\frac{k_N}{k_\sigma} \left| \langle \chi_- | \chi_\sigma \rangle t_{\sigma\sigma'}^{(-)} + \langle \chi_+ | \chi_\sigma \rangle t_{\sigma\sigma'}^{(+)} \right|^2 \right] \quad (19)$$

$$\approx \text{Re} \left[\frac{k_N}{k_\sigma} \left| \langle \chi_- | \chi_\sigma \rangle t_{\sigma\sigma'}^{(-)} \right|^2 \right] \equiv T_{\sigma\sigma'}^{(-)},$$

where $\sigma' = \pm\sigma$ corresponds to transmissions without and with spin-flip, respectively. We also define the magnitude of the residue $T_{\sigma\sigma'}^{(+)} \equiv \text{Re}[(k_N/k_\sigma) |\langle \chi_+ | \chi_\sigma \rangle t_{\sigma\sigma'}^{(+)}|^2]$, which indicates the accuracy of the approximation.

For clarity, the following analysis is based on the small P . We focus on the states with k_{\parallel} satisfying the open channel condition k_{\parallel}^0 , recall Eqs. (11) and (12). In such cases, the barrier is almost transparent and we can assume the reflection is negligible. Therefore, under this approximation, by introducing a modified \hat{H}'_B , such that $\hat{H}_B = \hat{H}'_B d\delta(z)$ [recall Eq. (3)], we obtain, $\hat{H}'_B \psi_{\sigma'}^{(-)}(0) \approx \hat{H}'_B \langle \chi_- | \chi_\sigma \rangle \chi_- = 0$, which means $Z_{\text{eff}}^- = 0$, see Eqs. (11).

The condition that determines the k_{\parallel} of the open channels is only affected by the barrier parameters. The reason that we have k_F , q_F in the open channel condition is that Z , λ are the dimensionless quantities that are defined with the effective mass and wave vectors. The open channel condition can also be written as $V_0 = \alpha k_{\parallel}/d$, which remains the same when the effective masses and Fermi wave vectors are different in the F and N regions.

For a large barrier and strong SOC, Z , $\lambda \gg 1$, the maximum transmission condition become $Z = \lambda k_{\parallel}/(2\sqrt{k_F q_F})$, which is consistent with the proposed open channel condition, k_{\parallel}^0 from Eq. (12). We notice

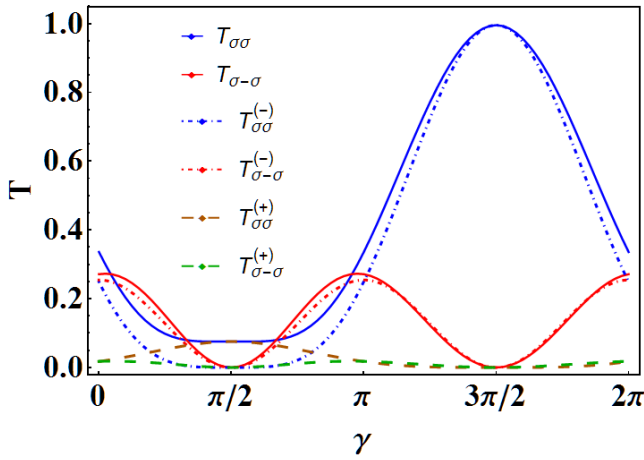


FIG. 5. Comparison of the approximate ($T_{\sigma\sigma'}^{(-)}$) and accurate ($T_{\sigma\sigma'}$) results for transmissions at the open channels, where $\lambda=5$, $Z = 1.5$, $P = 0.2$, $k_{\parallel} = 0.6k_F$, $\sigma = 1$ and $\mathbf{M}_{\parallel} - \mathbf{y}$. $T_{\sigma\sigma'}^{(+)}$ are the magnitude of the residue.

that the wave vectors on both sides can only change the magnitude of the transmission, rather than the condition for its maximum, when the barrier is large enough. Therefore, introducing unequal Fermi wave vectors will not affect the open channel condition. This conclusion also applies to the systems with different effective masses on both sides.

Now we can solve the system without any barrier and obtain the approximate transmissions. For in-plane \mathbf{M} , $\theta = \pi/2$ and $|\langle \chi_- | \chi_\sigma \rangle|^2 = (1/2)[1 - \sigma \sin(\gamma - \phi)]$. Thus the total transmission at the open channel is given by Eq. (13), with

$$T_{\sigma\sigma} = \frac{k_\sigma k_N [1 - \sigma \sin(\gamma - \phi)]^2}{(k_\sigma + k_N)^2}, \quad (20)$$

$$T_{\sigma-\sigma} = \begin{cases} \frac{k_N (k_\sigma + k_{-\sigma})^2 \cos^2(\gamma - \phi)}{4k_\sigma (k_N + k_{-\sigma})^2}, & k_{-\sigma} \in \mathbb{R}, \\ \frac{k_N (k_\sigma^2 + |k_{-\sigma}|^2) \cos^2(\gamma - \phi)}{4k_\sigma (k_N^2 + |k_{-\sigma}|^2)}, & k_{-\sigma} \in i\mathbb{R}. \end{cases} \quad (21)$$

Figure 5 shows the comparison between the accurate and approximate results. Two facts can be noticed: (i) The transmission from the component with spinor χ_+ is negligible, so the approximation in Eq. (19) is valid. (ii) The transmissions for a simple F/N junction without any barrier agree well with the accurate ones and thus Eqs. (20) and (21), obtained using this model, are valid. The different patterns of open channels in Fig. 3 of the main text can now be understood. Since the transmission without the spin flip, $T_{\sigma\sigma} \propto [1 - \sigma \sin(\gamma - \phi)]^2$, has a 2π period, it forms a single crescent shape of open channels. In contrast, the spin-flip transmission, $T_{\sigma-\sigma} \propto \cos^2(\gamma - \phi)$, has a period of π and thus forms two crescents.

We can also calculate the transmissions for out-of-plane \mathbf{M} . In this case, $|\langle \chi_- | \chi_\sigma \rangle|^2 = 1/2$ and there is no ϕ dependence due to the rotational symmetry. The total transmission at a certain open channel is then given by Eq. (13), with

$$T_{\sigma\sigma} = \frac{k_\sigma k_N}{(k_\sigma + k_N)^2}, \quad (22)$$

$$T_{\sigma-\sigma} = \begin{cases} \frac{k_N (k_\sigma + k_{-\sigma})^2}{4k_\sigma (k_N + k_{-\sigma})^2}, & k_{-\sigma} \in \mathbb{R}, \\ \frac{k_N (k_\sigma^2 + |k_{-\sigma}|^2)}{4k_\sigma (k_N^2 + |k_{-\sigma}|^2)}, & k_{-\sigma} \in i\mathbb{R}. \end{cases} \quad (23)$$

When P is small, we can find the ratio between the transmission with and without spin flip $T_{\sigma-\sigma}/T_{\sigma\sigma} = 1 +$

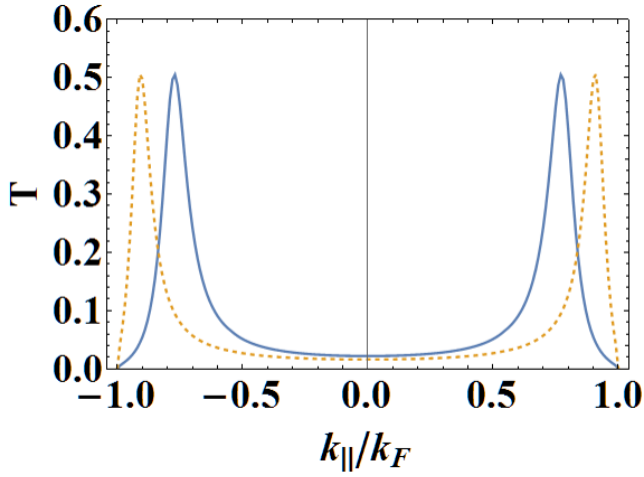


FIG. 6. Comparison of the open channel positions at the maximum conductance between accurate numerical (solid) and approximate analytical (dashed) results, where $\lambda = 20$, $Z = 7.6$ (solid), $Z = 8.9$ (dashed), $P = 0.7$, $\sigma, \sigma' = 1$ and $\mathbf{M} \parallel \mathbf{z}$.

$P^2 / \left[4 \left(1 - k_{\parallel}^2 / k_F^2 \right) \right]^2 + O(P^4) \approx 1$, and thus we can estimate the total transmission for the incident particle with spin σ and $k_{\parallel} = k_{\parallel}^{\sigma}$, using

$$T_{\sigma} = \frac{2\sqrt{1 + \sigma P - k_{\parallel}^2 / k_F^2} \sqrt{1 - k_{\parallel}^2 / k_F^2}}{\left(\sqrt{1 + \sigma P - k_{\parallel}^2 / k_F^2} + \sqrt{1 - k_{\parallel}^2 / k_F^2} \right)^2}. \quad (24)$$

This result also applies to the average transmission for open channels with in-plane \mathbf{M} .

Most of the conductance comes from the open channels and their neighborhoods (quasi-open channels), i.e., $k_{\parallel} \in [(2Z/\lambda)k_F - \Delta k/2, (2Z/\lambda)k_F + \Delta k/2]$ with Δk the width of the open channels. Therefore, to obtain maximum conductance, we need both a large amount of open channels and small mismatch between the wave vectors. As a result, we need to maximize the following normalized conductance,

$$G_{\sigma}(Q) = \frac{2\pi Q k_F \Delta k T_{\sigma}}{(2\pi k_F^2)} = \frac{\Delta k}{k_F} \frac{2Q \sqrt{1 + \sigma P - Q^2} \sqrt{1 - Q^2}}{\left(\sqrt{1 + \sigma P - Q^2} + \sqrt{1 - Q^2} \right)^2}, \quad (25)$$

with respect to $Q = 2Z/\lambda$. For spin-up ($\sigma = 1$) incident electrons, we have $Q = 0.89$ with $P = 0.7$ and $Q = 0.94$ with $P = 0.2$. For spin-down ($\sigma = -1$) incident electrons, we have $Q = 0.46 = 0.83\sqrt{1 - P}$ with $P = 0.7$ and $Q = 0.83 = 0.93\sqrt{1 - P}$ with $P = 0.2$. These are the predicted conditions for Z and λ to achieve maximum conductance.

However, as can be seen from Fig. 6, for theoretically predicted conditions there is still some difference from

the accurate numerical results. The main reason is that we neglect the change of the open channel width with respect to its position. As it is shown in Fig. 6, when the open channels are too close to k_{\max} (see the main text), their width will decrease and a part of the expected quasi-open channels disappear due to $k_{\parallel} > k_{\max}$. Therefore, to avoid such losses, the distance between the open channels and k_{\max} is required to be greater than $\Delta k/2$. We introduce phenomenological correction W_1 (W_2) for spin-down (spin-up) incident electrons. These corrections depend on the spin polarization and barrier parameters. For $P = 0.2$ and $\lambda = 20$, we have $W_1 = 0.75$ for spin-down incident electrons and $W_2 = 0.87$ for spin-up ones. Considering all the corrections above, the parameter range giving the maximum conductance should be $W_1\sqrt{1 - P} < 2Z/\lambda < W_2$.

We note that these conditions for maximum conductance are different from the condition for a large ratio of the spin-triplet and spin-singlet contribution. In fact, the large triplet region starts just from the region of the vanishing singlet conductance and ends at the region for vanishing of the triplet one. Therefore, the condition for a large triplet contribution is $\sqrt{1 - P} < 2Z/\lambda < 1$.

* zigor@buffalo.edu

- [1] M. Eschrig, "Spin-polarized supercurrents for spintronics," *Phys. Today* **64**, 43 (2011).
- [2] J. Linder and J. W. A. Robinson, "Superconducting spintronics," *Nat. Phys.* **11**, 307 (2015).
- [3] W. M. Martinez, W. P. Pratt, Jr., and N. O. Birge, "Amplitude control of the spin-triplet supercurrent in S/F/S Josephson junctions," *Phys. Rev. Lett.* **116**, 077001 (2016).
- [4] D. Aasen, M. Hell, R. V. Mishmash, A. Higginbotham, J. Danon, M. Leijnse, T. S. Jespersen, J. A. Folk, C. M. Marcus, K. Flensberg, and J. Alicea, "Milestones toward Majorana-based quantum computing," *Phys. Rev. X* **6**, 031016 (2016).
- [5] A. Yu Kitaev, "Unpaired Majorana fermions in quantum wires," *Phys.-Usp.* **44**, 131 (2001).
- [6] V. Mourik, K. Zuo, S. M. Frolov, S. R. Plissard, E. P. A. M. Bakkers, and L. P. Kouwenhoven, "Signatures of Majorana fermions in hybrid superconductor-semiconductor nanowire devices," *Science* **336**, 1003 (2012).
- [7] L. P. Rokhinson, X. Liu, and J. K. Furdyna, "The fractional a.c. Josephson effect in a semiconductor-superconductor nanowire as a signature of Majorana particles," *Nat. Phys.* **8**, 795 (2012).
- [8] A. P. Mackenzie and Y. Maeno, "The superconductivity of Sr_2RuO_4 and the physics of spin-triplet pairing," *Rev. Mod. Phys.* **75**, 657 (2003).
- [9] I. Žutić and I. Mazin, "Phase-sensitive tests of the pairing state symmetry in Sr_2RuO_4 ," *Phys. Rev. Lett.* **95**, 217004 (2005).
- [10] A. Pustogow, Y. Luo, A. Chronister, Y.-S. Su, D. A. Sokolov, F. Jerzembeck, A. P. Mackenzie, C. W. Hicks,

- N. Kikugawa, S. Raghu, E. D. Bauer, and S. E. Brown, “Constraints on the superconducting order parameter in Sr_2RuO_4 from oxygen-17 nuclear magnetic resonance,” *Nature* **574**, 72 (2019).
- [11] A. Steppke, L. Zhao, M. E. Barber, T. Scaffidi, F. Jerzembeck, H. Rosner, A. S. Gibbs, Y. Maeno, S. H. Simon, A. P. Mackenzie, and C. W. Hicks, “Strong peak in T_c of Sr_2RuO_4 under uniaxial pressure,” *Science* **355**, eaaf9398 (2017).
- [12] I. Žutić, A. Matos-Abiague, B. Scharf, H. Dery, and K. Belashchenko, “Proximitized materials,” *Mater. Today* **22**, 85 (2019).
- [13] T. Kontos, M. Aprili, J. Lesueur, and X. Grison, “Oscillations of the superconducting order parameter in a ferromagnet,” *Phys. Rev. Lett.* **86**, 304 (2001).
- [14] V. V. Ryazanov, V. A. Oboznov, A. Yu. Rusanov, A. V. Veretennikov, A. A. Golubov, and J. Aarts, “Coupling of two superconductors through a ferromagnet: Evidence for a π junction,” *Phys. Rev. Lett.* **86**, 2427 (2001).
- [15] L. Fu and C. L. Kane, “Superconducting proximity effect and Majorana fermions at the surface of a topological insulator,” *Phys. Rev. Lett.* **100**, 096407 (2008).
- [16] A. I. Buzdin, “Proximity effects in superconductor-ferromagnet heterostructures,” *Rev. Mod. Phys.* **77**, 935 (2005).
- [17] F. S. Bergeret, A. F. Volkov, and K. B. Efetov, “Odd triplet superconductivity and related phenomena in superconductor-ferromagnet structures,” *Rev. Mod. Phys.* **77**, 1321 (2005).
- [18] M. Eschrig, “Spin-polarized supercurrents for spintronics: A review of current progress,” *Rep. Prog. Phys.* **78**, 104501 (2015).
- [19] E. C. Gingrich, B. M. Niedzielski, J. A. Glick, Y. Wang, D. L. Miller, R. Loloee, W. P. Pratt, Jr., and N. O. Birge, “Controllable $0-\pi$ Josephson junctions containing a ferromagnetic spin valve,” *Nat. Phys.* **12**, 564 (2016).
- [20] A. Cottet, “Inducing odd-frequency triplet superconducting correlations in a normal metal,” *Phys. Rev. Lett.* **107**, 177001 (2011).
- [21] T. S. Khaire, M. A. Khasawneh, W. P. Pratt, Jr., and N. O. Birge, “Observation of spin-triplet superconductivity in Co-based Josephson junctions,” *Phys. Rev. Lett.* **104**, 137002 (2010).
- [22] J. W. A. Robinson, J. D. S. Witt, and M. G. Blamire, “Controlled injection of spin-triplet supercurrents into a strong ferromagnet,” *Science* **329**, 59 (2010).
- [23] A. Singh, S. Voltan, K. Lahabi, and J. Aarts, “Colossal proximity effect in a superconducting triplet spin valve based on the half-metallic ferromagnet CrO_2 ,” *Phys. Rev. X* **5**, 021019 (2015).
- [24] M. Alidoust and K. Halterman, Half-metallic superconducting triplet spin multivalves, *Phys. Rev. B* **97**, 064517 (2018), and the references therein.
- [25] R. S. Keizer, S. T. B. Goennenwein, T. M. Klapwijk, G. Miao, G. Xiao, and A. Gupta, “A spin triplet supercurrent through the half-metallic ferromagnet CrO_2 ,” *Nature* **439**, 825 (2006).
- [26] K.-R. Jeon, C. Ciccarelli, A. J. Ferguson, H. Kurebayashi, L. F. Cohen, X. Montiel, M. Eschrig, and J. W. A. Robinson M. G. Blamire, “Enhanced spin pumping into superconductors provides evidence for superconducting pure spin currents,” *Nat. Mater.* **17**, 499 (2018).
- [27] N. Banerjee, J. A. Ouassou, Y. Zhu, N. A. Stelmashenko, J. Linder, and M. G. Blamire, “Controlling the superconducting transition by spin-orbit coupling,” *Phys. Rev. B* **97**, 184521 (2018).
- [28] N. Satchell and N. O. Birge, “Supercurrent in ferromagnetic Josephson junctions with heavy metal interlayers,” *Phys. Rev. B* **97**, 214509 (2018).
- [29] L. G. Johnsen, J. Linder, and N. Banerjee, “Magnetisation reorientation due to superconducting transition in heavy metal heterostructures,” arXiv:1901.005001 (2019).
- [30] M. Duckheim and P. W. Brouwer, “Andreev reflection from noncentrosymmetric superconductors and Majorana bound-state generation in half-metallic ferromagnets,” *Phys. Rev. B* **83**, 054513 (2011).
- [31] R. M. Lutchyn, J. D. Sau, and S. Das Sarma, “Majorana fermions and a topological phase transition in semiconductor-superconductor heterostructures,” *Phys. Rev. Lett.* **105**, 077001 (2010).
- [32] Y. Oreg, G. Refael, and F. von Oppen, “Helical liquids and Majorana bound states in quantum wires,” *Phys. Rev. Lett.* **105**, 177002 (2010).
- [33] G. E. Blonder, M. Tinkham, and T. M. Klapwijk, “Transition from metallic to tunneling regimes in superconducting microconstrictions: Excess current, charge imbalance, and supercurrent conversion,” *Phys. Rev. B* **25**, 4515 (1982).
- [34] I. Žutić and S. Das Sarma, “Spin-polarized transport and Andreev reflection in semiconductor/superconductor hybrid structures,” *Phys. Rev. B* **60**, R16322 (1999).
- [35] I. Žutić, J. Fabian, and S. Das Sarma, “Spintronics: Fundamentals and applications,” *Rev. Mod. Phys.* **76**, 323 (2004).
- [36] S. Kashiwaya and Y. Tanaka, “Tunneling effects on surface bound states in unconventional superconductors,” *Rep. Prog. Phys.* **63**, 1641 (2000).
- [37] S. Wu and K. V. Samokhin, “Tunneling conductance of ferromagnet/noncentrosymmetric superconductor junctions,” *Phys. Rev. B* **80**, 014516 (2009).
- [38] P. Högl, A. Matos-Abiague, I. Žutić, and J. Fabian, “Magnetoanisotropic Andreev reflection in ferromagnet/superconductor junctions,” *Phys. Rev. Lett.* **115**, 116601 (2015).
- [39] F. S. Bergeret and I. V. Tokatly, “Singlet-triplet conversion and the long-range proximity effect in superconductor-ferromagnet structures with generic spin dependent fields,” *Phys. Rev. Lett.* **110**, 117003 (2013).
- [40] F. S. Bergeret and I. V. Tokatly, “Spin-orbit coupling as a source of long-range triplet proximity effect in superconductor-ferromagnet hybrid structures,” *Phys. Rev. B* **89**, 134517 (2014).
- [41] S. H. Jacobsen J. A. Ouassou and J. Linder, “Critical temperature and tunneling spectroscopy of superconductor-ferromagnet hybrids with intrinsic Rashba-Dresselhaus spin-orbit coupling,” *Phys. Rev. B* **92**, 024510 (2015).
- [42] M. Alidoust and K. Halterman, “Spontaneous edge accumulation of spin currents in finite-size two-dimensional diffusive spin-orbit coupled SFS heterostructures,” *New J. Phys.* **17**, 033001 (2015).
- [43] X. Montiel and M. Eschrig, “Generation of pure superconducting spin current in magnetic heterostructures via nonlocally induced magnetism due to Landau Fermi liquid effects,” *Phys. Rev. B* **98**, 104513 (2018).
- [44] I. Žutić and O. T. Valls, “Tunneling spectroscopy for ferromagnet/superconductor junctions,” *Phys. Rev. B* **61**,

- 1555 (2000).
- [45] J. Fabian, A. Matos-Abiague, C. Ertler, P. Stano, and I. Žutić, “Semiconductor spintronics,” *Acta Phys. Slovaca* **57**, 565 (2007).
- [46] A. Matos-Abiague and J. Fabian, “Anisotropic tunneling magnetoresistance and tunneling anisotropic magnetoresistance: Spin-orbit coupling in magnetic tunnel junctions,” *Phys. Rev. B* **79**, 155303 (2009).
- [47] R. J. Soulen Jr., J. M. Byers, M. S. Osofsky, B. Nadgorny, T. Ambrose, S. F. Cheng, P. R. Broussard, C. T. Tanaka, J. Nowak, J. S. Moodera, A. Barry, and J. M. D. Coey, “Measuring the spin polarization of a metal with a superconducting point contact,” *Science* **282**, 85 (1998).
- [48] J. Moser, A. Matos-Abiague, D. Schuh, W. Wegscheider, J. Fabian, and D. Weiss, “Tunneling anisotropic magnetoresistance and spin-orbit coupling in Fe/GaAs/Au tunnel junctions,” *Phys. Rev. Lett.* **99**, 056601 (2007).
- [49] I. Martinez, P. Högl, C. Gonzalez-Ruano, J. Pedro Cascales, C. Tiusan, Y. Lu, M. Hehn, A. Matos-Abiague, J. Fabian, I. Žutić, and F. G. Aliev, “Interfacial spin-orbit coupling: Platform for superconducting spintronics,” arXiv:1812.08090, *Phys. Rev. Applied* (in press) (2019).
- [50] I. Martinez, C. Tiusan, M. Hehn, M. Chshiev, and F. G. Aliev, “Symmetry broken spin reorientation transition in epitaxial MgO/Fe/MgO layers with competing anisotropies,” *Sci. Rep.* **8**, 9463 (2018).
- [51] K. V. Samokhin, “Symmetry and topology of two-dimensional noncentrosymmetric superconductors,” *Phys. Rev. B* **92**, 174517 (2015).
- [52] C.-T. Wu, O. T. Valls, and K. Halterman, “Tunneling conductance and spin transport in clean ferromagnet-ferromagnet-superconductor heterostructures,” *Phys. Rev. B* **90**, 054523 (2014).
- [53] Y. Miyoshi, Y. Bugoslavsky, and L. F. Cohen, “Andreev reflection spectroscopy of niobium point contacts in a magnetic field,” *Phys. Rev. B* **72**, 012502 (2005).
- [54] H. T. Simensen and J. Linder, “Tunable superconducting critical temperature in ballistic hybrid structures with strong spin-orbit coupling,” *Phys. Rev. B* **97**, 054518 (2018).
- [55] P. H. Barsic and O. T. Valls, “Tunneling conductance in superconductor/ferromagnet junctions: Self-consistent approach,” *Phys. Rev. B* **79**, 014502 (2009).
- [56] O. T. Valls, M. Bryan, and I. Žutić, “Superconducting proximity effects with a repulsive pairing interaction,” *Phys. Rev. B* **82**, 134534 (2010).
- [57] A. Costa, P. Högl, and J. Fabian, “Magnetoelectric Josephson effect due to interfacial spin-orbit fields in superconductor/ferromagnet/superconductor junctions,” *Phys. Rev. B* **95**, 024514 (2017).
- [58] R. Beiranvand, H. Hamzeshpour, and M. Alidoust, “Tunable anomalous Andreev reflection and triplet pairings in spin-orbit-coupled graphene,” *Phys. Rev. B* **94**, 125415 (2016).
- [59] P. Lv, Y.-F. Zhou, N.-X. Yang, and Q.-F. Sun, “Magnetoelectric spin-triplet Andreev reflection in ferromagnet-Ising superconductor junctions,” *Phys. Rev. B* **97**, 144501 (2018).
- [60] M. M. Desjardins, L. C. Contamin, M. R. Delbecq, M. C. Dartiaill, L. E. Bruhat, T. Cubaynes, J. J. Viennot, F. Mallet, S. Rohart, A. Thiaville, A. Cottet, and T. Kontos, “Synthetic spin orbit interaction for Majorana devices,” *Nat. Mater.* **18**, 1060 (2019).
- [61] G. L. Fatin, A. Matos-Abiague, B. Scharf, and I. Žutić, “Wireless Majorana bound states: From magnetic tunability to braiding,” *Phys. Rev. Lett.* **117**, 077002 (2016).
- [62] A. Matos-Abiague, J. Shabani, A. D. Kent, G. L. Fatin, B. Scharf, and Žutić, “Tunable magnetic textures: From Majorana bound states to braiding,” *Solid State Commun.* **262**, 1 (2017).
- [63] J. Klinovaja, P. Stano, A. Yazdani, and D. Loss, “Topological superconductivity and Majorana fermions in RKKY systems,” *Phys. Rev. Lett.* **111**, 186805 (2013).
- [64] G. Yang, P. Stano, J. Klinovaja, and D. Loss, “Majorana bound states in magnetic skyrmions,” *Phys. Rev. B* **93**, 224505 (2016).
- [65] T. Zhou, N. Mohanta, J. E. Han, A. Matos-Abiague, and I. Žutić, “Tunable magnetic textures in spin valves: From spintronics to Majorana bound states,” *Phys. Rev. B* **99**, 134505 (2019).
- [66] U. Güngördü, S. Sandhoefner, and A. A. Kovalev, “Stabilization and control of Majorana bound states with elongated skyrmions,” *Phys. Rev. B* **97**, 115136 (2018).
- [67] N. Mohanta, T. Zhou, J. Xu, J. E. Han, A. D. Kent, J. Shabani, I., and A. Matos-Abiague, “Electrical control of Majorana bound states using magnetic stripes,” *Phys. Rev. Applied* **12**, 034048 (2019).
- [68] A. Yazdani, “Conjuring Majorana with synthetic magnetism,” *Nat. Mater.* **18**, 1036 (2019).
- [69] M. Garnier, A. Mesaros, and P. Simon, “Topological superconductivity with deformable magnetic skyrmions,” *Commun. Phys.* **2**, 126 (2019).
- [70] S. S. P. Parkin, C. Kaiser, A. Panchula, P. M. Rice, B. Hughes, M. Samant, and S.-H. Yang, “Giant tunneling magnetoresistance at room temperature with MgO (100) tunnel barriers,” *Nat. Mater.* **3**, 862 (2004).
- [71] S. Yuasa, T. Nagahama, A. Fukushima, Y. Suzuki, and K. Ando, “Giant room-temperature magnetoresistance in single-crystal Fe/MgO/Fe magnetic tunnel junctions,” *Nat. Mater.* **3**, 868 (2004).